AIAA AVIATION Forum
August 2-6, 2021, VIRTUAL EVENT
AIAA AVIATION 2021 FORUM

10.2514/6.2021-2581

Design of 3D Co-Flow Jet Airfoil with Integrated Micro-Compressor for High Operating Efficiency at Cruise Condition

Paula A. Barrios * Yan Ren † Kewei Xu ‡ GeCheng Zha §
Dept. of Mechanical and Aerospace Engineering
University of Miami, Coral Gables, Florida 33124
E-mail: gzha@miami.edu

June 28, 2021

Abstract

This paper conducts a design study for a 3D Co-Flow Jet (CFJ) airfoil at Mach 0.25 with integrated micro-compressor. The purpose is to let the micro-compressor operate at the high efficiency range at the cruise condition. The CFJ airfoil is designed first to achieve an optimal cruise efficiency to meet the mission requirements with the required dimension (chord). A micro-compressor is then designed to satisfy the required total pressure ratio and the dimension of the airfoil with maximized mass flow rate. The CFJ injection and suction ducts are then designed with minimum total pressure loss and to match the high efficiency operating region in the compressor map. The ducts connecting the micro-compressor with the 3D CFJ airfoil have a circular shape at the interface with the micro-compressor and then transition to rectangle slots at the airfoil. Duct design iteration is a crucial step in the integration of the CFJ airfoil with micro-compressor by matching mass flow rate and compressor total pressure ratio to the high efficiency operating region. The micro-compressor outlet is simulated with a swirl profile provided from the compressor design. The design is for the cruise condition at angle of attack 5° with a range of ±5°. Results show that by integration of micro-compressor and CFJ airfoil through duct design, an operating range at cruise for the CFJ airfoil system is achieved with excellent micro-compressor efficiency from 79% to 85%. The study indicates that CFJ airfoil design integration with the micro-compressor is able to make the CFJ aircraft cruise at a high efficiency operating range of the compressor.

Nomenclature

CFJ	Co-flow jet
AoA	Angle of attack
LE	Leading edge
TE	Trailing edge
S	Planform area
c	Airfoil chord
U	Flow velocity
q	Dynamic pressure $0.5\,\rho\,U^2$
p	Static pressure
η	Compressor efficiency

* Ph.D. Candidate
† PostDoc Researcher. Ph.D., AIAA member
‡ Ph.D. Candidate
§ Professor, ASME Fellow, AIAA associate Fellow

ρ	Air density
$\dot{m}$	Mass flow rate
M	Mach number
ω	Pitching moment
P	Pumping power
SD	Suction duct
ID	Injection duct
∞	Free stream conditions
j	Jet conditions
C_L	Lift coefficient $L/(q_\infty S)$
C_D	Drag coefficient $D/(q_\infty S)$
C_M	Moment coefficient
C_μ	Jet momentum coefficient $\dot{m}_j U_j /(q_\infty S)$
$(C_L/C_D)_c$	CFJ airfoil corrected aerodynamic efficiency
$(C_L^2/C_D)_c$	CFJ airfoil productivity efficiency
P_{act}	Actual power consumed by the micro-compressor P_C/η
P_C	Power coefficient $L/(q_\infty S V_\infty)$
P_P	Propeller Actuator power coefficient $\frac{2}{\rho V_\infty^3 S}\sqrt{\frac{F^3}{2\rho A}}$
P_R	Total pressure ratio between injection and suction
M_∞	Free stream Mach number
$P_{t,inj}$	Total injection pressure
$P_{t,suc}$	Total suction pressure
V_{inj}/V_∞	Normalized injection velocity

1 Introduction

Minimizing energy consumption centers on high cruise efficiency, especially in creating electric aircraft where it is important to extend range and payload with limited battery energy density. Active flow control (AFC) is promising to enhance aerodynamic performance. However, increasing aircraft aerodynamic efficiency at cruise condition is challenging because the flow is typically benign at low angle of attack. Enhancing cruise efficiency requires that the AFC have low energy expenditure with high conversion efficiency. Most of the efforts to improve cruise efficiency are made by passive flow controls, including winglet, wing body combination, flying wing configurations, boundary layer ingestion, distributed propulsion, etc. Not much progress has been made to improve subsonic airfoil cruise efficiency by AFC.

AFC is to transfer external energy to the controlled flow in order to improve the performance of the flow system. For all AFC systems, there are three measures of merit (MoM): 1) effectiveness, 2) power required (PR), and 3) power conversion efficiency (PCE). Effectiveness quantifies the performance enhancement, e.g., removal of flow separation, drag reduction, lift increase, stall prevention, noise mitigation, etc. Power required quantifies the AFC power needed to achieve the targeted effectiveness. Power conversion efficiency quantifies the efficiency to convert the external energy (e.g., mechanical, electric, chemical) to the energy required by the controlled flow. It determines how much total power will be consumed by the actual flow control system. For an AFC to benefit industry realistic applications, all three MoM matter. The ultimate criterion for an AFC is that the system efficiency gain should be greater than the AFC energy expenditure.

The Co-Flow Jet (CFJ) airfoil is a zero-net mass-flux (ZNMF) AFC method developed by Zha et al. [1, 2, 3, 4, 5, 6, 7, 8, 9, 10, 11] that can dramatically increase the lift coefficient, stall angle of attack, and drag reduction. For the CFJ AFC, a small amount of mass flow is withdrawn into the suction duct near the TE, pressurized and energized

by the micro-compressor, and injected near the LE tangentially to the main flow through the injection slot. The low energy expenditure required by the CFJ enables it to improve cruise productivity efficiency, $C_L^2/(C_D + P_C)$ substantially compared with the conventional design (P_C is the required power coefficient). In other words, CFJ is proved to have high effectiveness and low power required. The actual power consumed by the micro-compressor is $P_{act} = P_C/\eta$, where η is the compressor power conversion efficiency. This paper focuses on the third MoM: improving the power conversion efficiency, which is to make the CFJ airfoil at cruise operate at a high efficiency region of the compressor map.

The CFJ AFC relies on the micro-compressor actuators to convert the mechanical power to the power required [12]. However, the first effort made by Zha et al. in [12] had the compressor operate at near choking conditions with low efficiency due to lack of design integration. To achieve high power conversion efficiency, it is important that the CFJ airfoil operating conditions match the micro-compressor operating line with high efficiency. This requires that the design of the CFJ airfoil be integrated with the micro-compressors as concluded by Zha et al. [12] and Xu et al. [13]. The purpose of this paper is to numerically design and simulate an integrated CFJ airfoil with micro-compressor in order to achieve high system energy conversion efficiency at Mach number 0.25.

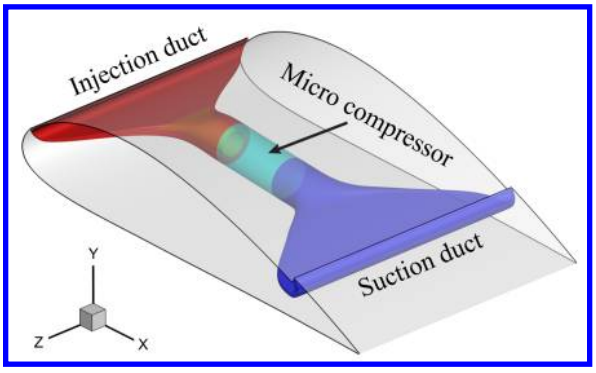

Figure 1: Schematic of CFJ setup within the airfoil

2 Methodology

2.1 Lift and Drag Calculation

In a CFD analysis, the total aerodynamic force and moments are determined by the force surface integral and jet reactionary force. The reactionary force of a CFJ airfoil is calculated through flow parameters obtained from the injection and suction slots. The equations for lift and drag due to the jet reactionary force are given by Zha et al. [2] using the control volume analysis in Figure 2:

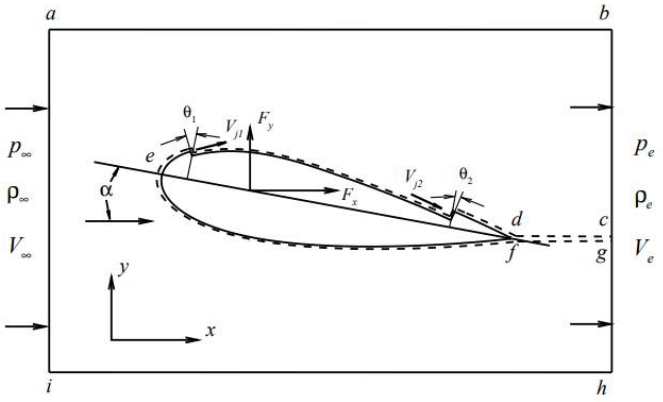

Figure 2: Control volume of a CFJ airfoil

$$F_{x_{cfj}} = (\dot{m}_j V_{j1} + p_{j1} A_{j1}) * cos(\theta_1 - \alpha) - (\dot{m}_j V_{j2} + p_{j2} A_{j2}) * cos(\theta_2 + \alpha) \tag{1}$$

$$F_{y_{cfj}} = (\dot{m}_{j1} V_{j1} + p_{j1} A_{j1}) * sin(\theta_1 - \alpha) + (\dot{m}_{j2} V_{j2} + p_{j2} A_{j2}) * sin(\theta_2 + \alpha) \tag{2}$$

where the subscript 1 indicates the injection slot and subscript 2 denotes the suction slot, θ_1 and θ_2 are the angles between the slot's surface and a line normal to the chord. α is the angle of attack.

Total lift and drag are given by the following equations:

$$D = R'_x - F_{x_{cfj}} \tag{3}$$

$$L = R'_y - F_{y_{cfj}} \tag{4}$$

where R'_x and R'_y are surface integrals of pressure and shear stress in the x_{drag} and y_{lift} directions. For a 3D CFJ wing, total lift and drag are determined by integrating the drag and lift equations in the span wise direction.

2.2 Jet Momentum Coefficient

C_μ, or the jet momentum coefficient, quantifies the jet intensity and is defined by,

$$C_\mu = \frac{\dot{m} V_j}{\frac{1}{2} \rho_\infty {V_\infty}^2 S} \tag{5}$$

where $\dot{m}$ is the injection mass flow rate, V_j is the mass-averaged injection velocity, ρ_∞ is the free stream density, V_∞ is the free stream velocity, and S is the planform area.

2.3 Power Coefficient

In a CFJ airfoil, a system of micro-compressors are embedded inside of the wing. The compressors take air from the suction slot and and eject the air through the injection slot. The power consumption is determined by the jet mass flow and total enthalpy change through:

$$P_{CFJ} = \dot{m}(H_{t1} - H_{t2}) \tag{6}$$

where H_{t1} and H_{t2} are the mass-averaged total enthalpy in the injection and suction slots, P is the power required by the micro-compressor and $\dot{m}$ the jet mass flow rate. The power consumption of Eq. (6) can be also expressed by the following equation,

$$P_{CFJ} = \frac{\dot{m} C_p T_{t2}}{\eta} (\Gamma^{\frac{\gamma-1}{\gamma}} - 1) \tag{7}$$

where γ is the specific heat ratio, or 1.4 for ideal gas, η is the isentropic pumping efficiency. Γ is the total pressure ratio of the pump defined as $\Gamma = \frac{P_{t1}}{P_{t2}}$, where P_{t1} and P_{t2} are the mass-averaged total pressures in the injection and suction slots, respectively. The power coefficient for a CFJ airfoil is then,

$$P_{C,CFJ} = \frac{P_{CFJ}}{\frac{1}{2}\rho_\infty V_\infty^3 S} \tag{8}$$

The power coefficient for a propeller actuator is given by,

$$P_P = \frac{2}{\rho V_\infty^3 S} \sqrt{\frac{F^3}{2\rho A}} \tag{9}$$

where F is the total force generated by the propeller actuator perpendicular to the propeller disk, and A is the area of the actuator disk. The propeller power coefficent can also be given by the absolute value of the drag coefficient because the propeller thrust is to overcome the drag at cruise.

The power coefficient due to CFJ and the propeller actuator can be combined as,

$$P_C = P_{C,CFJ} + P_P \tag{10}$$

2.4 Corrected Aerodynamic Efficiency

For a conventional airfoil, the wing aerodynamic efficiency is defined as:

$$\frac{L}{D} \tag{11}$$

and for a CFJ wing, the pure aerodynamic relationship between lift and drag still follows Eq. (11). However, since CFJ AFC expends energy, the above is modified to consider the energy consumption of the micro-compressor. The propeller actuator must also be taken into account. The corrected aerodynamic efficiency is:

$$\frac{C_L}{C_{Dc}} = \frac{C_L}{C_D + P_C} \tag{12}$$

where C_{Dc} is the equivalent drag coefficient that includes the drag of the aircraft system and the power required by the propeller and CFJ. At cruise, since the propeller thrust exactly offsets the drag, the C_D is equal to 0 in Eq.(12).

2.5 Aircraft Productivity

The productivity efficiency C_L^2/C_D is used to measure the productivity of an airplane characterized by the product of an aircraft's range and its weight [14]. It is a more thorough parameter than C_L/C_D in determining the merit of aerodynamic design during cruise. Aircraft productivity includes the ratio of lift to drag coefficient and the aircraft weight from C_L. The corrected productivity efficiency for CFJ airfoils with propeller actuator is defined as,

$$\frac{C_L^2}{C_{Dc}} = \frac{C_L^2}{C_D + P_C} \tag{13}$$

2.6 Airfoil Geometry

The CFJ 6421 airfoil used has the injection and suction slot size normalized by airfoil chord length (C). The CFJ6421-SST150-SUC247-INJ117 with an injection slot size of 1.17%C and suction slot size of 2.47%C [15, 16, 17] is used as the initial design. However, during design iterations, the suction slot was decreased by 15% to reduce flow separation. The airfoil used in this study is then CFJ6421-SST150-SUC205-INJ117. The airfoil is developed based on the NACA 6421 airfoil.

2.7 Duct Geometry

The ducts have a circular shape at the compressor interface and then become rectangular at the slots. The method of calculating circular-to-rectangular transition surfaces developed in [18] is adopted. The CFJ airfoil injection and suction slot locations are determined according to previously published 2D design [15, 16, 17]. The injection and suction duct meanlines are determined based on the slot locations. Superellipses are created along those duct meanlines, which pass through the superellipse geometric centers and locally perpendicular to the superellipses. The duct surfaces are formed by connecting those cross sections.

Converging ducts have a favorable pressure gradient and are easier to design than diverging ducts which are prone to flow separation. When designing the injection duct, the center body design is important since it is used to guide the swirl flow exiting the micro-compressor and prevents flow separation. Key parameters in suction duct design are the area and width of the duct.

Duct design is an integral part of consolidation of the system, requiring as high a possible total pressure recovery and healthy flow throughout. Total pressure recovery is defined as,

$$P_{tr} = \frac{\oiint_{S_o} \rho V P_{02} dA}{\oiint_{S_i} \rho V P_{01} dA} \tag{14}$$

where S_o and S_i are the cross section interface at outlet and inlet respectively. P_{02} and P_{01} are the total pressure evaluated at outlet and inlet. A high total pressure recovery signifies little loss within the duct. For injection ducts, the total pressure decreases toward the injection slot while for suction ducts the total pressure decreases toward the compressor interface. In general, the total pressure recovery of injection ducts is smaller than suction ducts due to the swirl flow and center body increasing energy loss [18].

2.8 CFD Simulation Setup

The FASIP (Flow-Acoustics-Structure Interaction Package) CFD code is used for the numerical simulation. The 3D Reynolds Averaged Navier-Stokes (RANS) equations with one-equation Spalart-Allmaras [19] turbulence model is used. A 3rd order WENO scheme for the inviscid flux [20, 21, 22, 23, 24, 25] and a 2nd order central differencing for the viscous terms [21] are utilized to discretize the Navier-Stokes equations. The low diffusion E-CUSP scheme used as the approximate Riemann solver suggested by Zha et al. [21] is utilized with the WENO scheme to evaluate the inviscid fluxes. Implicit time marching method using Gauss-Seidel line relaxation is used to achieve a fast convergence rate [26]. Parallel computing is implemented to save wall clock simulation time [27].

2.9 Boundary Conditions

The 3rd order accuracy no slip condition is enforced on the solid surface with the wall treatment suggested in [28] to achieve the flux conservation on the wall. The computational mesh is shown in Fig. 6. Symmetric boundary conditions are utilized on the two boundaries in the span direction. Total pressure, total temperature and flow angles are specified at the injection duct inlet based on the profile of the micro-compressor at the outlet. The total pressure, total temperature, and flow angle are also specified at the upstream portion of the far field based on free stream condition. Constant static pressure is applied at the suction duct outlet as well as the downstream portion

of the far field. The actuator disk boundary condition is modeled as a flat surface with a specified pressure jump, the forces are iterated so that the sum of forces in the x direction is 0. The total mesh size is 5.68 million points, split into 135 blocks for the parallel computation. The first grid point on the wing surface is placed at $y^+ \approx 1$.

3 Results and Discussion

3.1 Steps for the Integrated Design

The integrated design steps are the following:

1. CFJ wing design: 2D CFJ airfoil and 3D CFJ wing are designed to meet the aircraft mission requirement for takeoff, cruise, and landing with optimal performance. The design provides the requirements of wing dimensions, micro-compressor mass flow rate, and total pressure ratio.

2. Micro-compressor design: A micro-compressor is then designed to satisfy the required total pressure ratio and the dimensions of the airfoil with maximized mass flow rate, highest efficiency, and largest operating range from choke limit to stall limit.

3. Duct design: The CFJ injection and suction ducts are then designed to match the airfoil dimensions with the boundary conditions from the micro-compressor and the CFJ wing flow conditions, no flow separation inside the ducts, and minimum total pressure loss.

4. Integrate the ducts with the 3D CFJ airfoil using the micro-compressor flow conditions at the CFJ injection inlet (micro-compressor outlet) and suction outlet (micro-compressor inlet). Simulate the 3D CFJ airfoil with the ducts designed in Step 3.

5. Examine the results and the aerodynamic performance. If satisfied, stop; if not satisfied, return to Step 1 and repeat the process.

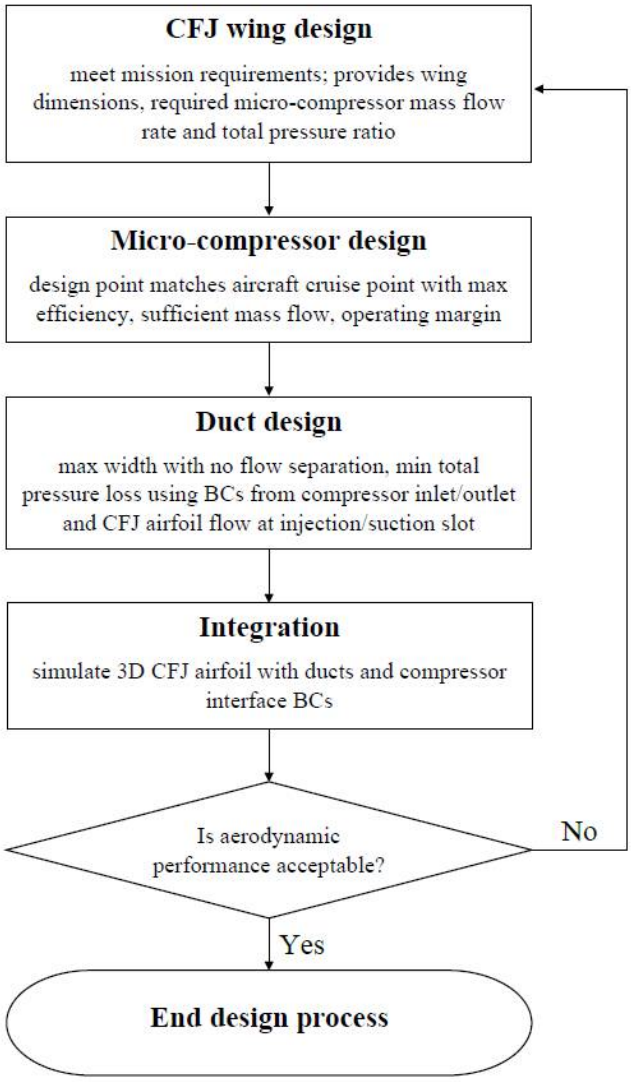

Figure 3: Flowchart of the integrated design process

3.2 The Micro-Compressor

Cruise Mach number 0.25 is studied in this paper for a potential electric CFJ aircraft cruise condition. The total pressure loss is small, with the total pressure ratio required for the micro-compressor at cruise condition being about 1.015. The micro-compressor designed is named G8A. The following table summarizes the normalized design point performance while Figure 4 displays the configuration of the G8A micro-compressor including the inlet, impeller, stator, and outlet.

Table 1: Design point performance of micro-compressor G8A used for Mach number 0.25

	$\overline{\dot{m}}$	P_{tr}	η
G8A	1	1.04	84%

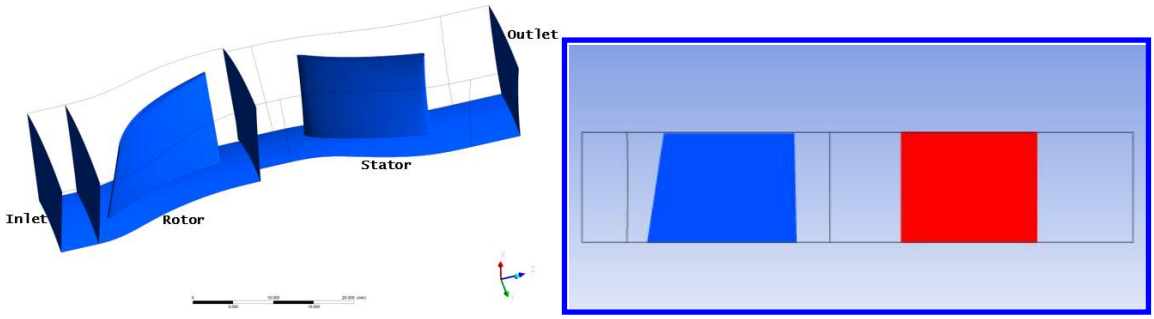

Figure 4: Configuration of the G8A micro-compressor

Figure 5 shows the micro-compressor design point Mach number contours at three different span locations of the impeller and stator, 10%, 50%, and 90% span. The maximum Mach number, 0.437, is near the rotor tip and the flow is not choked.

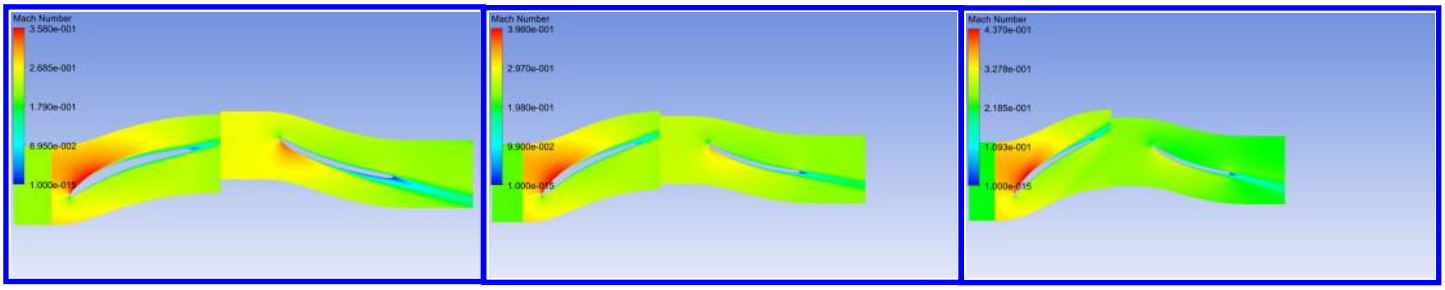

(a) (b) (c)

Figure 5: Mach number contours of the rotor and stator at (a)10%, (b)50%, and (c)90% span

3.3 CFJ Injection and Suction Ducts

In order to integrate the micro-compressor with the CFJ airfoil, the injection and suction ducts should be designed with the following requirements:

1. Match the mass flow requirement for the required C_μ
2. No flow separation inside the ducts to minimize the total pressure loss and maximize the flow uniformity at the injection slot
3. Maximize the slot width to minimize the number of micro-compressors to be used. However, a large ratio of slot width to compressor diameter, W/D, will also make the flow easier to separate.

The injection duct in the present design is converging while the suction duct is diverging. Figure 6 shows the mesh used for the ducts and the suction surface of the airfoil. The ducts designed for $M = 0.25$ have a W/D ratio of 2.76 for both injection and suction; each duct has a mesh size of 1.62 million points, split into 20 blocks. The injection and suction ducts have a total pressure recovery of 98.78% and 99.1% respectively, shown in Figure 7.

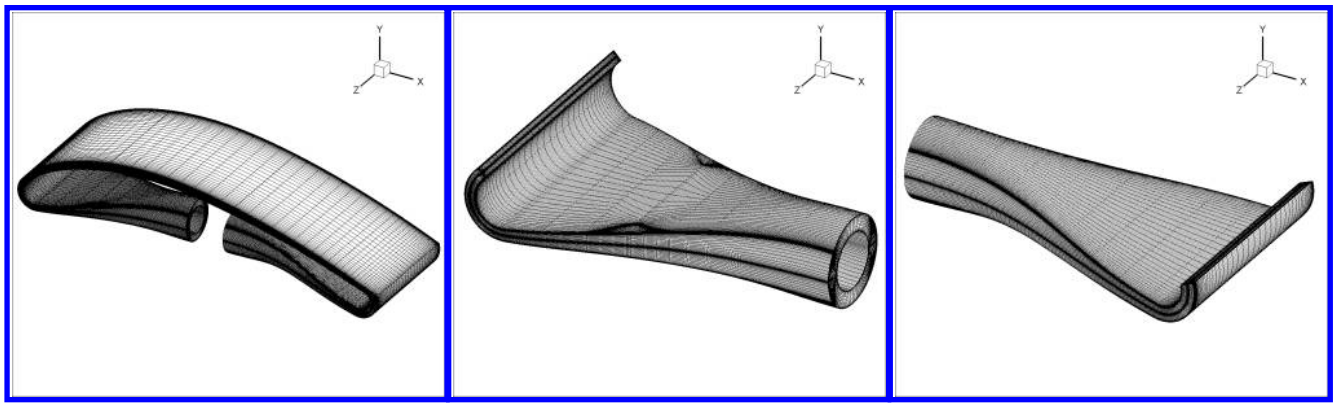

Figure 6: Computational mesh of airfoil surfaces and ducts used for $M = 0.25$

2D Mach contours and streamlines are shown in Figure 8 for the injection and suction ducts. Contours of the injection duct show the flow is attached throughout the duct with the Mach number at the injection slot fairly uniform. The streamlines clearly display the swirl effects due to the micro-compressor. The suction duct shows very healthy flow through out except at the top of the duct near the micro-compressor interface where there is a very small low Mach number region. Flow is generally strong in the majority area of the duct because of the centrifugal forces at the turn near the inlet that push flow to the bottom. Upon further inspection of the design suction duct, however, the streamlines do not show any separation. The suction designed was deemed acceptable to continue with due to the high total pressure recovery.

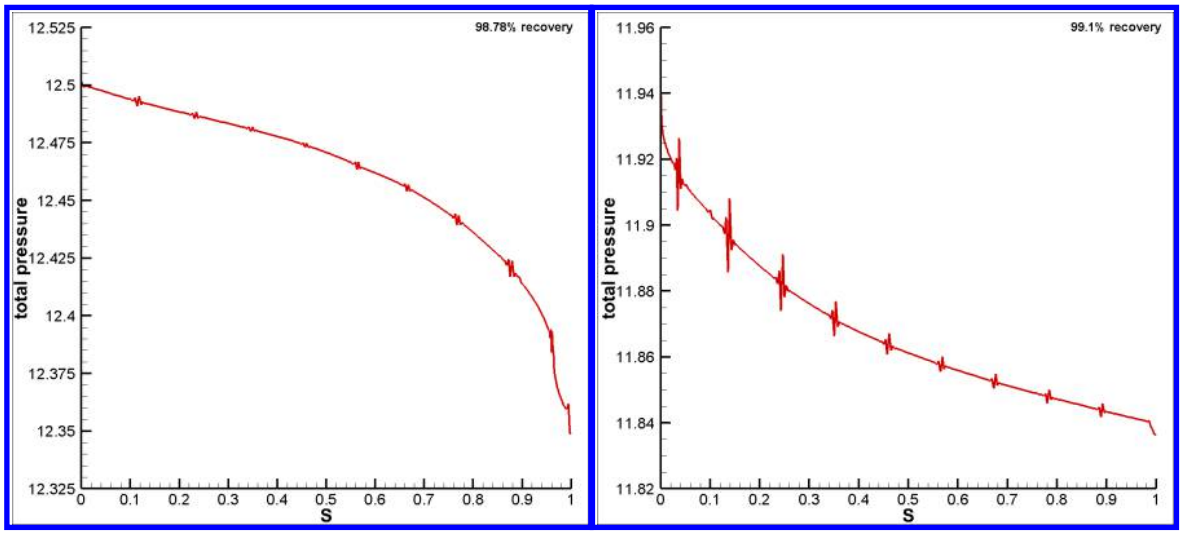

(a) (b)

Figure 7: Total pressure distribution for (a)injection and (b)suction duct designed for CFJ airfoil using G8A micro-compressor at Mach number 0.25

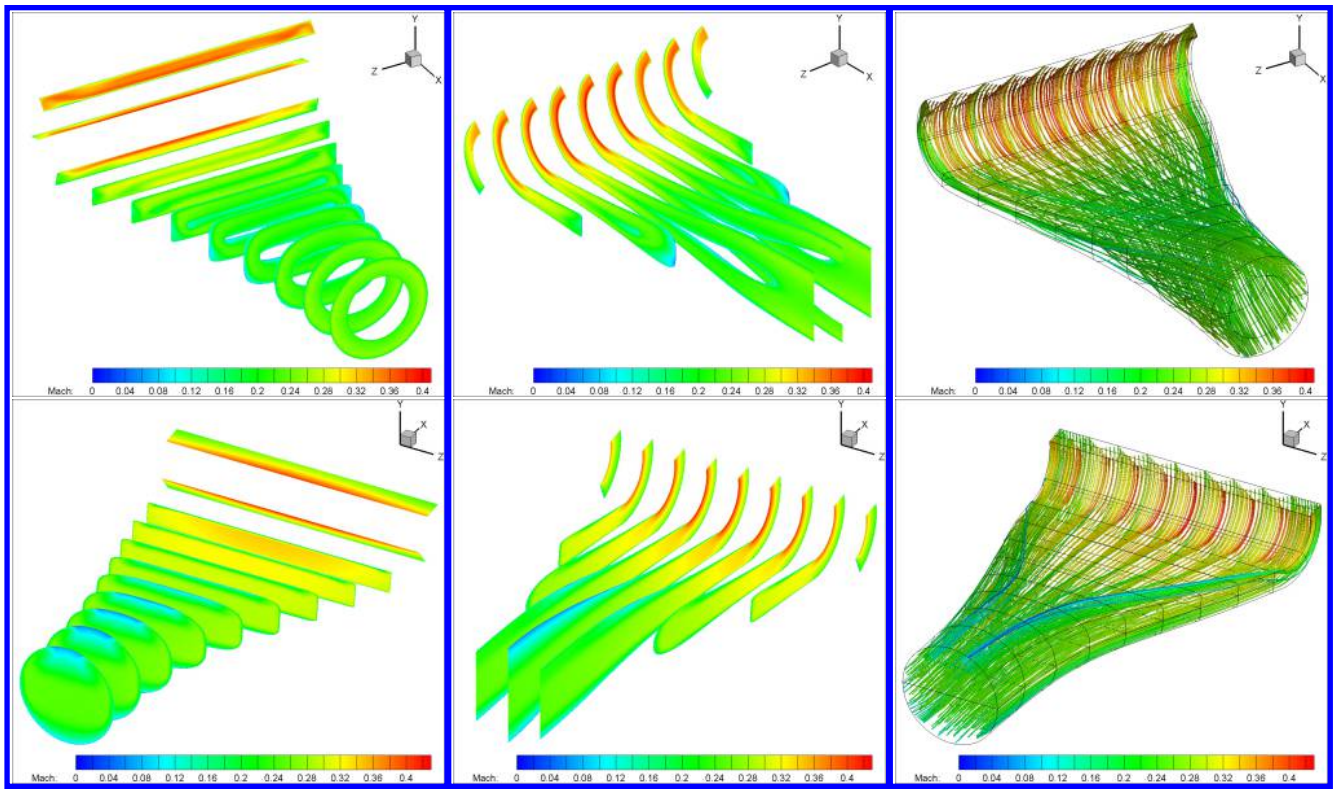

Figure 8: 2D Mach contours and streamlines at top row: injection duct, bottom row: suction duct, for CFJ airfoil using G8A micro-compressor at Mach number 0.25

3.4 Integration of the Micro-Compressor with CFJ Airfoil

After the injection and suction duct design is completed, they are integrated with the 3D CFJ airfoil to simulate the whole flow field with the external flow and the duct internal flow. The results of the numerical simulation analysis are shown below.

Table 2 lists the performance of cruise Mach number 0.25 at different angles of attack using G8A micro-compressor. AoA of 0° and 5° were simulated at a C_μ of 0.03 as per [17, 29], however, at AoA 10° the jet momentum coefficient had to be increased to 0.06 to remove flow separation occurring on the suction surface. Values of P_C indicate the total power coefficients of the CFJ airfoil and the propeller actuator. In Table 2, the drag coefficient is equal to the propeller power coefficient because at cruise the thrust is equal to the drag. If referring to Eq. (12), $C_D = 0$. The highest CFJ corrected aerodynamic efficiency, 74.094, occurs at AoA 5°. This is very close to the results observed by Wang et al. [17] for a 2D CFJ airfoil with rectangular ducts at Mach number 0.3. Results indicate that the micro-compressor will work at an operating point with an efficiency of 79% for the cruise point, a very desirable performance. In fact, for all the simulated angles of attack, the micro-compressor performs at high efficiency, proving that a closely coupled CFJ airfoil design with compressor design will result in optimal performance at their operating conditions.

Figure 9 shows the compressor stage map at different RPM of the G8A micro-compressor along with the operating conditions of the CFJ airfoil. For the same C_μ, as AoA increases from 0° to 5°, the mass flow slightly decreases because the jet velocity is slightly increased due to the higher leading edge suction peak effect. But, with C_μ increased to 0.06 for AoA of 10°, the mass flow and the total pressure ratio increase. The operating conditions of the CFJ airfoil at $M = 0.25$ all fall within the high efficiency operating range of the micro-compressor and show that the integrated system can operate at high compressor efficiency.

Table 2: Performance at $M = 0.25$ for different AoA with G8A micro-compressor

Mach	AoA	C_μ	C_L	P_C	C_L/C_{Dc}	C_L^2/C_{Dc}	P_{tr}	$\overline{\dot{m}}$	η
0.25	0°	0.03	0.825	0.0196	42.024	34.661	1.051	1.0159	85%
	5°	0.03	1.321	0.0178	74.094	97.850	1.027	0.9912	79%
	10°	0.06	1.915	0.0359	53.297	102.07	1.053	1.3691	80%

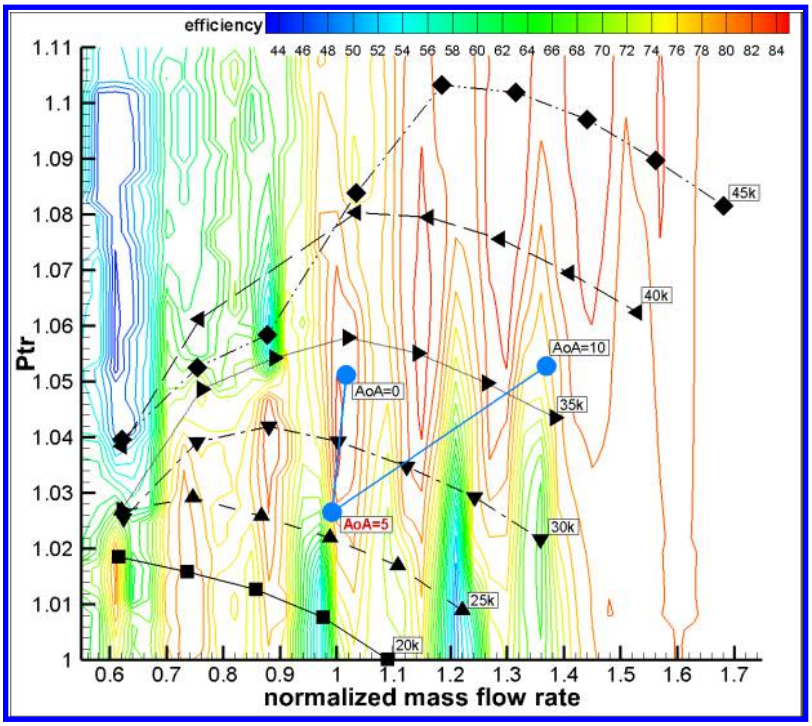

Figure 9: Compressor map of G8A micro-compressor with operating conditions of CFJ airfoil at different AoA for Mach number 0.25

The flow field of the CFJ airfoil at the 50% span wise location for AoA 5° for Mach number 0.25 is shown in Figure 10(a). The maximum Mach number is 0.42 for $M = 0.25$. The flow field is attached to the airfoil. The suction surface shows some small flow non-uniformity, which is created by the swirl flow coming out of the compressor. However, the overall flow performs very well. The Mach contours at 50% span wise show the suction duct outlet having a low Mach number region at the top half of the duct, but the streamlines along the ducts and suction surface do not show any flow separation. Figure 10(c) and (d) show some of the flow from the inlet far field (the colored streamlines) merging with the flow from the injection duct (the black streamlines) and both going into the suction duct. The flow going into the suction duct is mixed between the injection jet and the main flow as shown by the streamlines in black and in color. A comparison of Figure 10(a) and (c) shows that the flow from the injection jet is more on the top of the suction duct with low energy due to the boundary layer loss (streamlines in black), whereas the flow from the main stream is more thrown to the bottom of the duct (in color) due to the centrifugal force at the turning of the suction duct.

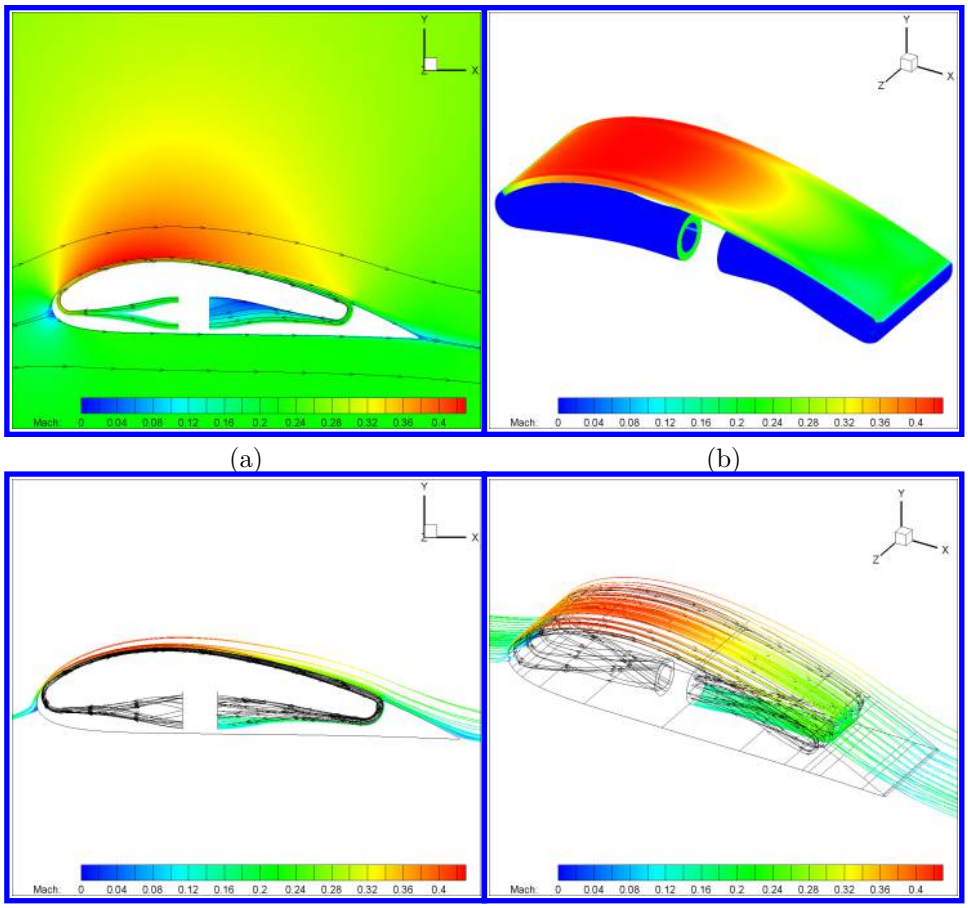

Figure 10: (a)Mach contour flow field of the CFJ airfoil at 50% span wise location, (b)Mach contour of designed ducts and suction surface, (c) and (d) far field and injection duct streamlines merging into suction duct at AoA=5° with G8A micro-compressor for $M = 0.25$

4 Conclusion

This paper conducts a design study for a 3D Co-Flow Jet (CFJ) airfoil at Mach 0.25 with integrated micro-compressor. The purpose is to let the micro-compressor operate at the high efficiency range at the cruise condition. The CFJ airfoil is designed first to achieve an optimal cruise efficiency to meet the mission requirements with the required dimension (chord). A micro-compressor is then designed to satisfy the required total pressure ratio and the dimension of the airfoil with maximized mass flow rate. The CFJ injection and suction ducts are then designed with minimum total pressure loss and to match the high efficiency operating region in the compressor map. The ducts connecting the micro-compressor with the 3D CFJ airfoil have a circular shape at the interface with the micro-compressor and then transition to rectangle slots at the airfoil. Duct design iteration is a crucial step in the integration of the CFJ airfoil with micro-compressor by matching mass flow rate and compressor total pressure ratio to the high efficiency operating region. The micro-compressor outlet is simulated with a swirl profile provided from the compressor design. The design is for the cruise condition at angle of attack 5° with a range of ±5°. Results show that by integration of micro-compressor and CFJ airfoil through duct design, an operating range at cruise for the CFJ airfoil system is achieved with excellent micro-compressor efficiency from 79% to 85%. The study indicates that CFJ airfoil design integration with the micro-compressor is able to make the CFJ aircraft cruise at a high efficiency operating range of the compressor.

5 Acknowledgement

The authors would like to acknowledge the computing resource provided by the Center of Computational Sciences at the University of Miami. The teaching assistantship support from the University of Miami is acknowledged.

Disclosure: The University of Miami and Dr. Gecheng Zha may receive royalties for future commercialization of the intellectual property used in this study. The University of Miami is also equity owner in CoFlow Jet, LLC, licensee of the intellectual property used in this study.

References

[1] G. Zha, and C.D. Paxton, "A Novel Flow Control Method for Airfoil Performance Enhancement Using Co-Flow Jet," *Applications of Circulation Control Technologies, AIAA Book Series, Progress in Aeronautics and Astronautics*, vol. Vol. 214, Chapter 10, pp. 293–314, 2006.

[2] G. Zha, W. Gao, and C.D. Paxton, "Jet Effects on Co-Flow Jet Airfoil Performance," *AIAA Journal*, vol. 45, pp. 1222–1231, 2007.

[3] G.-C. Zha, C. Paxton, A. Conley, A. Wells, and B. Carroll, "Effect of Injection Slot Size on High Performance Co-Flow Jet Airfoil," *AIAA Journal of Aircraft*, vol. 43, pp. 987–995, 2006.

[4] G.-C. Zha, B. Carroll, C. Paxton, A. Conley, and A. Wells, "High Performance Airfoil with Co-Flow Jet Flow Control," *AIAA Journal*, vol. 45, pp. 2087–2090, 2007.

[5] Wang, B.-Y. and Haddoukessouni, B. and Levy, J. and Zha, G.-C., "Numerical Investigations of Injection Slot Size Effect on the Performance of Co-Flow Jet Airfoil," *Journal of Aircraft*, vol. Vol. 45, No. 6,, pp. pp.2084–2091, 2008.

[6] B. P. E. Dano, D. Kirk, and G.-C. Zha, "Experimental Investigation of Jet Mixing Mechanism of Co- Flow Jet Airfoil." AIAA-2010-4421, 5th AIAA Flow Control Conference, Chicago, IL, 28 Jun - 1 Jul 2010.

[7] B. P. E. Dano, G.-C. Zha, and M. Castillo, "Experimental Study of Co-Flow Jet Airfoil Performance Enhancement Using Micro Discreet Jets." AIAA Paper 2011-0941, 49th AIAA Aerospace Sciences Meeting, Orlando, FL, 4-7 January 2011.

[8] A. Lefebvre, B. Dano, W. Bartow, M. Fronzo, and G. Zha, "Performance and energy expenditure of coflow jet airfoil with variation of mach number," *Journal of Aircraft*, vol. 53, no. 6, pp. 1757–1767, 2016.

[9] A. Lefebvre and G. Zha, "Numerical simulation of pitching airfoil performance enhancement using co-flow jet flow control," vol. 2517, 2013.

[10] A. Lefebvre and G. Zha, "Co-flow jet airfoil trade study part i : Energy consumption and aerodynamic performance," vol. 2682, 2014.

[11] A. Lefebvre and G. Zha, "Co-flow jet airfoil trade study part ii : Moment and drag," vol. 2683, 2014.

[12] G.-C. Zha, Y.-C. Yang, Y. Ren, and B. McBreen, "Super-lift and thrusting airfoil of coflow jet-actuated by micro-compressors." AIAA Paper 2017-3061, AIAA AVIATION 2018, Atlanta, GA, Submitted for publication in AIAA Journal , 25 - 29 June 2018.

[13] K. Xu, B. McBreen, Y. Ren, and G.-C. Zha, "Analysis of micro-compressor performance with integrated co-flow jet airfoil ducting system." AIAA Paper 2017-3061, AIAA SciTech Forum, Orlando, FL, January 6-10, 2020.

[14] Yang, Yunchao and Zha, Gecheng, "Super-Lift Coefficient of Active Flow Control Airfoil: What is the Limit?," *AIAA Paper 2017-1693, AIAA SCITECH2017, 55th AIAA Aerospace Science Meeting, Grapevine, Texas*, p. 1693, 9-13 January 2017.

[15] Y. Wang and G.-C. Zha, "Study of 3D Co-flow Jet Wing Induced Drag and Power Consumption at Cruise Conditions." AIAA Paper 2019-0034, AIAA SciTech 2019, San Diego, CA, January 7-11, 2019.

[16] Y. Wang, Y.-C. Yang, and G.-C. Zha, "Study of Super-Lift Coefficient of Co-Flow Jet Airfoil and Its Power Consumption." AIAA Paper 2019-3652, AIAA Aviation 2019, AIAA Applied Aerodynamics Conference, Dallas, Texas, 17-21 June 2019.

[17] Y. Wang and G.-C. Zha, "Study of Mach Number Effect for 2D Co-Flow Jet Airfoil at Cruise Conditions." AIAA Paper 2019-3169, AIAA Aviation 2019, AIAA Applied Aerodynamics Conference, Dallas, Texas, 17-21 June 2019.

[18] Y. Ren and G.-C. Zha, "Design of Injection and Suction Ducts for Co-Flow Jet Airfoils with Embedded Micro-Compressors Actuator." AIAA Aviation Forum, 2018 Flow Control Conference, Atlanta, Georgia, 25-29 June 2018.

[19] P. R. Spalart and S. R. Allmaras, "A one-equation turbulence model for aerodynamic flows," in *30th Aerospace Sciences Meeting and Exhibit, Aerospace Sciences Meetings, Reno, NV, USA, AIAA Paper 92-0439*, 1992.

[20] Shen, Y.Q., and Zha, G.C., "Large Eddy Simulation Using a New Set of Sixth Order Schemes for Compressible Viscous Terms," *Journal of Computational Physics*, vol. 229, pp. 8296–8312, doi:10.1016/j.jcp.2010.07.017, 2010.

[21] Zha, G.C., Shen, Y.Q. and Wang, B.Y., "An improved low diffusion E-CUSP upwind scheme ," *Journal of Computer and Fluids*, vol. 48, pp. 214–220, Sep. 2011.

[22] Y.-Q. Shen and G.-Z. Zha , "Generalized finite compact difference scheme for shock/complex flowfield interaction," *Journal of Computational Physics*, vol. doi:10.1016/j.jcp.2011.01.039, 2011.

[23] Shen, Y.Q., Zha, G.C., and Wang, B.Y., "Improvement of Stability and Accuracy of Implicit WENO Scheme," *AIAA Journal*, vol. 47, pp. 331–334, DOI:10.2514/1.37697, 2009.

[24] Shen, Y.Q., Zha, G.C., and Chen, X., "High Order Conservative Differencing for Viscous Terms and the Application to Vortex-Induced Vibration Flows," *Journal of Computational Physics*, vol. 228(2), pp. 8283–8300, doi:10.1016/j.jcp.2009.08.004, 2009.

[25] Shen, Y.Q., and Zha, G.C., "Improvement of the WENO Scheme Smoothness Estimator," *International Journal for Numerical Methods in Fluids*, vol. 64,, pp. 653–675, DOI:10.1002/fld.2186, 2009.

[26] Zha, G.C., and Bilgen, E., "Numerical Study of Three-Dimensional Transonic Flows Using Unfactored Upwind Relaxation Sweeping Algorithm," *Journal of Computational Physics*, vol. 125, pp. 425–433,, 1996.

[27] Wang, B.Y., Hu, Z. and Zha, G.C., "A General Sub-Domain Boundary Mapping Procedure For Structured Grid CFD Parallel Computation," *AIAA Journal of Aerospace Computing, Information, and Communication*, vol. 5, pp. 425–447, 2008.

[28] Y.-Q. Shen, G.-C. Zha, and B.-Y. Wang, "Improvement of Stability and Accuracy of Implicit WENO Scheme," *AIAA Journal*, vol. 47, pp. 331–344, 2009.

[29] Y. Wang and G.-C. Zha, "Study of Mach Number Effect for 3D Co-Flow Jet Wings at Cruise Conditions." AIAA Paper 2020-0045, AIAA SciTech 2020, AIAA SciTech 2020 Forum, Orlando, Florida, 6-10 January 2020.